Principal components in three-ball cascade juggling

Post, A.A.; Daffertshofer, A.; Beek, P.J.

published in
Biological Cybernetics
2000

DOI (link to publisher)
10.1007/PL00007966

document version
Publisher's PDF, also known as Version of record

Biol. Cybern. 82, 143–152 (2000)

Biological Cybernetics

Principal components in three-ball cascade juggling

A.A. Post, A. Daffertshofer, P.J. Beek

Faculty of Human Movement Sciences, Vrije Universiteit, Van der Boechorststraat 9, 1081 BT Amsterdam, The Netherlands
Institute for Fundamental and Clinical Human Movement Sciences, Amsterdam/Nijmegen

Received: 1 April 1999 / Accepted in revised form: 9 August 1999

Abstract. To uncover the underlying control structure of three-ball cascade juggling, we studied its spatiotemporal properties in detail. Juggling patterns, performed at fast and preferred speeds, were recorded in the frontal plane and subsequently analyzed using principal component analysis and serial correlation techniques. As was expected on theoretical grounds, the principal component analysis revealed that maximally four instead of the original six dimensions (3 balls $\times$ 2 planar coordinates) are sufficient for describing the juggling dynamics. Juggling speed was shown to affect the number of dimensions (four for the fast condition, two for the preferred condition) as well as the smoothness of the time evolution of the eigenvectors of the principal component analysis, particularly around the catches. Contrary to the throws and the zeniths, and regardless of juggling speed, consecutive catches of the same hand showed a markedly negative lag-one serial correlation, suggesting that the catches are timed so as to preserve the temporal integrity of the juggling act.

1 Introduction

Randomness is an inherent feature of biological systems. The combination of deterministic processes with random fluctuations results in a stochastic system that may be measured by its degree of variability. Variability in this sense is a hallmark property of human motor performance. Depending on one's theoretical perspective, it has been perceived as a curse or as a blessing. On the one hand, additional stochasticity can limit the "prediction horizon" of an operational measure, i.e., randomness can reduce the controllability of a system. On the other hand, random fluctuations can also play a beneficial role. For instance, viewing motor control as an optimization problem, they may be useful to avoid spurious states, i.e., locally stable states in which the system might get trapped. Random fluctuations can provide escapes from such undesired states and, thus, support the search for the global optimum. Similarly, random fluctuations may be required to induce switches from one state to another (cf. critical fluctuations, e.g., Haken 1983; Gardiner 1990; Kelso 1995) or may lead to resonance phenomena (cf. stochastic resonance, e.g., Benzi et al. 1981; Jung and Hänggi 1991; Hu Gang et al. 1996). Recent studies also considered the case of noise-induced stabilization of unstable orbits (Wackerbauer 1998). Even in the absence of such dynamical aspects, stochasticity may generate correlations between observables that may provide a window into the underlying control structure. For example, statistically independent noise sources, defined by clock and motor variances, produce error corrections in terms of negative serial correlations (Wing and Kristofferson 1973; Vorberg and Wing 1996; Thaut et al. 1998). In summary, variability should be viewed as an intrinsic and essential property of human movement systems and may be exploited to obtain vital information about the control structure of these systems (Shannon and Weaver 1949; Haken 1988). The question is how.

Usually, the description of a process by means of a small number of variables is based on a priori assumptions regarding the most relevant events in the data obtained. In studying human movement, such events might be the start of a limb movement, sign reversals in the acceleration or velocity profiles, or the moment at which the aperture of the thumb and the index finger is maximal in a prehension task. The inherent danger of this approach is that, in the study of a certain task, particular events may be falsely assumed to be relevant, whereas more important features of the dynamics may be ignored. For instance, Haggard and Wing (1997) found that the thumb is a more appropriate control index in prehension than the wrist, which has been used in many studies as the main variable of interest. To avoid such unpleasant discoveries, methods for analysis are needed that address the entire set of time series and

Correspondence to: A.A. Post (e-mail: a_a_post@fbw.vu.nl, Tel.: +31-20-4448454, Fax: +31-20-4448509)

allow for the detection of the most significant events without presupposing them.

To the extent that such methods exist, they capitalize on the intrinsic variability of natural phenomena. Various operational measures of variability (spectral analyses, cross-correlations, dimensionality analyses, Gestalt methods, etc.) can be applied. Unfortunately, the most commonly used estimates are standard deviations or other scalar values with a limited analytical scope. Certainly, the standard deviation is a useful measure of variability, assuming the underlying distribution is sufficiently symmetric. However, it does not provide information about possible correlations between subsequent observations of the same variable or between different variables. It may be the case that successive data points are not simple random fluctuations about a mean value. Correlations within the dynamics of an individual variable can be measured by its corresponding auto-correlation function. If the dynamics pertain to a few distinct points in time, it is expedient to consider the auto-correlation function only at these points leading to (discrete) serial lag correlations. An estimate of the number of relevant variables, however, requires a study of the cross-correlations between different time series. To account for such correlations in time, one can consider the system's (cross-)covariance matrix. The principal component analysis (also known as Karhunen-Loève expansion or singular value decomposition) is a particularly powerful tool to decompose complex distributed signals into lower-dimensional structures. Such lower-dimensional structures may be more amenable to an analysis of the underlying dynamics than the original pattern itself. In spite of its wide application in physics, engineering and biology (e.g., Fuchs et al. 1992; Oja 1992), this tool has seldom been applied to human movement. A notable exception is the analysis of pedalo riding movements (Haas 1995; Haken 1996), which revealed that the original 22-dimensional whole-body movement vector could be reduced to five or fewer dimensions. This reduction allowed for the study of changes in dimensionality in the course of learning to ride the pedalo, which turned out to occur predominantly in the arm movements.

In the present paper, we apply the aforementioned methods to gain insight into the control structure of three-ball cascade juggling. Juggling has proven to be a very useful experimental task for studying the dynamical properties of human perceptual-motor organizations (Beek 1989; Beek and Turvey 1992; Beek and Van Santvoord 1992; Beek and Lewbel 1995). The significance of juggling for the present context resides in the fact that a juggler, i.e., a highly dimensional control system, has to accommodate rather severe task constraints in order to juggle successfully. In view of this requirement, it is to be expected that a small number of relevant principal components are sufficient to describe the entire spatiotemporal pattern of (cascade) juggling.

Juggling is a cyclic activity in which the hands move along more or less elliptical trajectories while throwing and catching balls in a regular fashion (Beek 1989; Van Santvoord 1995). In cascade juggling, one hand moves clockwise and the other anti-clockwise (Fig. 1) with an average phase difference of circa 180°. The balls are, in this particular pattern, released at the inside of the ellipses and caught at the outside. Between throws and catches, they travel through the air to the other hand along a parabolic trajectory. Figure 1 depicts the paths of the moving hands and balls in the frontal plane. It is worth noting that there is one point where the ball trajectories intersect, and where they can collide when badly timed.

Van Santvoord and Beek (1996) examined the variability of both spatial and temporal juggling variables. With respect to the spatial variables, it was found that the dispersion of the points of release was smaller than that of the zeniths, which, in turn, was smaller than that of the catches. With respect to the temporal variables, it was found that the variability of ball flight intervals was smaller than that of loaded hand intervals, which, in turn, was smaller than that of empty hand intervals. Furthermore, the temporal variability of full ball cycle intervals (i.e., from catch to catch) was smaller than that of full hand cycle intervals. These findings were interpreted by viewing juggling as a "spatial clock": By throwing the balls consistently to a specific height, jugglers set up a stable time base for the hand movements. However, Van Santvoord and Beek (1996) only studied variability at discrete points of the movement. The analyses offered here build on their findings by focusing on the entire time-dependent trajectories. To gain insight into the patterns of variability, linear analysis techniques such as cross-spectral and relative-phase analysis will be applied. Without presupposing distinct sources of variability identified as discrete events during the task (throw, catch, etc.), they can emerge depending on the specific task constraints. Provided that this occurs, further correlation analyses will be used to explore specific control features (e.g., error correction).

Movement frequency has been demonstrated to be a control parameter in many motor tasks, affecting the stability of performance. In doing so, it can induce qualitative changes in behavior. These changes may be readily observable in the form of a qualitative change in the performed pattern, but they may also be more subtle. In juggling, task constraints are so severe that a bifurcation to a pattern with different phasing characteristics is not to be expected. However, increase in frequency

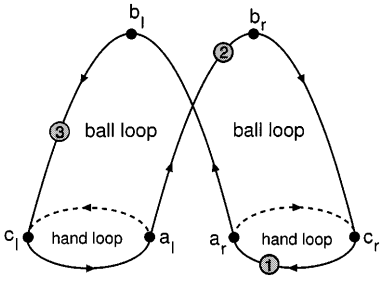

Fig. 1. Paths of the three balls and the two hands during cascade juggling. Between throw ($a_{l,r}$) and catch points ($c_{l,r}$) the balls describe a parabolic path which peaks at b_l, while the hands (subscripts l, r) follow a more or less elliptic path

induces an increase in variability of throwing location and the corresponding throw velocity vector and results consequently in a more variable parabolic flight path. This may have implications for the way in which task control is brought about. Thus, two juggling frequency levels were used to investigate the influence of frequency on task performance.

2 Experiment

2.1 Methods

2.1.1 Subjects

Four jugglers of intermediate skill who could not juggle more than three balls in a cascade pattern participated in the experiment. All subjects were right-handed and had normal or corrected-to-normal vision. They were paid a small fee for their participation.

2.1.2 Experimental setup

A 16-mm high-speed motion picture camera (DBM 55, Teledyne Camera Systems, Arcadia, Calif.) was used for data collection. The focus of the zoom lens was adjusted so that the juggler and the entire juggling pattern were in view of the camera. A flashing light with a fixed frequency was placed in view of the camera to check the actual frame rate against the nominal frame rate (125 Hz). The gravitational vertical was defined by a plumb line suspended from the ceiling. Proper lighting conditions for filming were created with the help of four 2000-W stage lamps. The equipment of the subject consisted of three so-called stage balls (diameter 7.3 cm, mass 130 g).

2.1.3 Procedure

Subjects were placed in front of the camera at a distance of about 5 m, which was sufficient to avoid significant distortions of the image on the projection plane of the film. They were asked to juggle the balls in cascade fashion, either at a preferred or at a fast frequency (i.e., markedly faster than preferred). Before the start of each trial, the subject was allowed to juggle a few cycles to accommodate to the task instructions in question. When the subject reported that a satisfactory juggle was achieved, the movie camera was started. During each trial, roughly 22 complete juggling cycles were recorded.

2.2 Pre-processing

After development, the films (Kodak 7251, Ektachrome high-speed daylight film, 400 ASA) were projected onto the opaque screen of a film-motion analyzer (NAC type MC OF) by means of a 16-mm projector (NAC type RH 160F), connected to a computer. The position of the projector was adjusted so as to align the plumb line visible on the film with the vertical axis of the projection screen. Frame by frame, the horizontal and vertical coordinates of the centers of the balls were digitized. Thus, each ball trajectory was represented by a two-dimensional time series $[x_j(t), y_j(t)]$ with $j = 1, 2, 3$. For each trial, these time series were rescaled to the interval $[-1, 1]$ by subtracting their mean and dividing by their maximal value.

3 Data analysis

During cascade juggling, a 90° rotated figure-8 movement pattern is generated (Fig. 2, left panel). In the course of a full revolution of a ball to its original position (e.g., a left-hand catch), the ball travels once from left to right and vice versa while it travels twice along a parabolic flight path. This can be viewed as 1:2 frequency locking between the horizontal and vertical components of each ball trajectory (Fig. 2, right panel). Furthermore, the balls are juggled equidistantly in time, which can be viewed as phase locking between the balls.

From the moment a ball leaves a hand, it follows a simple ballistic path until it is caught by the other hand $[y \sim (x - x_0)^2 \sim (t - t_{0,i})^2$; see Fig. 3]. To determine the individual flight intervals, we therefore fitted the flight trajectories of the balls to a parabola.

Throws (a_r and a_l) and catches (c_r and c_l) were identified at the points at which the trajectories deviated more than 5% (relative to the maximal displacement of the ball) from the estimated parabola. The parabolas in question were determined with the help of the zeniths (b_l and b_r) of the ball flight (see Figs. 1, 3). In addition, the corresponding temporal variables were determined, that is, the moments at which these spatial locations were reached (t_a, t_b, and t_c).

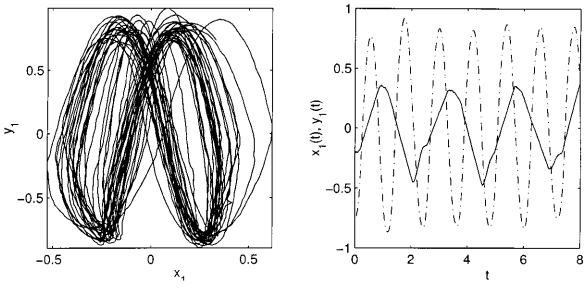

Fig. 2. Example of the recorded ball trajectories. The cascade juggling pattern (*left panel*) consists of individual ball trajectories composed of a horizontal evolution $x_k(t)$ and a vertical evolution $y_k(t)$ (*right panel*). $x_k(t)$ (*solid line*) oscillates with half the frequency as $y_k(t)$ (*dash-dotted line*)

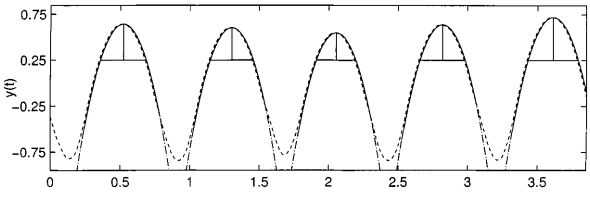

Fig. 3. *y*-Component of the trajectory of one ball (*dashed*); piecewise parabolic fit (*dash-dotted*)

3.1 Spatiotemporal analysis

In three-ball cascade juggling, the individual trajectories of the balls can be considered as (largely) identical but phase-shifted by $2\pi/3$. Such symmetries reflect the existence of some redundancy in the acquired signals that can be eliminated by transforming the system onto its principal axes. For this sake, we merged the trajectories of the three balls and described each data set by a six-dimensional signal $\boldsymbol{q}(t) := [x_1(t), y_1(t), x_2(t), y_2(t), x_3(t), y_3(t)]^T$. For a lower-dimensional approximation of the data, we chose an optimal set of vectors $\{\boldsymbol{v}_k\}$ to obtain

$$\boldsymbol{q}(t) \approx \sum_{k=1}^{M<6} \xi_k(t)\boldsymbol{v}_k \quad . \tag{1}$$

The choice of the basis vectors $\boldsymbol{v}_k$ was realized by minimizing the least square error

$$\mathscr{E}_M := \left\langle \left[\boldsymbol{q}(t) - \sum_{k=1}^{M} \xi_k(t)\boldsymbol{v}_k \right]^2 \right\rangle \stackrel{!}{=} \min \quad . \tag{2}$$

In Eq. (2), $\langle\cdot\rangle$ denotes the time average given by $\langle\cdot\rangle = 1/T \int_0^T [\cdot]\mathrm{d}t$, where T is the length of the time series and t denotes time. In this approach, the vectors $\boldsymbol{v}_k$ are assumed to be pairwise orthogonal so that the minimization of $\mathscr{E}_M$ becomes equivalent to an iterative construction of vectors along the direction of maximal variance of the data. This is followed by a subtraction of the remaining subspace via projection (Karhunen 1946). The iteration is truncated after M steps and realized by diagonalizing the covariance matrix $\underline{\boldsymbol{R}}$ of the data set $\boldsymbol{q}(t) = [q_1(t), \ldots, q_6(t)]^T$. The components of the so obtained matrix are explicitly defined as

$$R_{mn} \propto \langle Q_m(t) Q_n(t) \rangle \quad \text{with } Q_i(t) := q_i(t) - \langle q_i(t) \rangle \quad , \tag{3}$$

and further rescaled by means of $\mathrm{tr}(\underline{\boldsymbol{R}}) \equiv 1$. The eigenvectors of the covariance matrix define the desired vectors $\boldsymbol{v}_k$. The corresponding eigenvalues λ_k reflect the amount of signal (variance) that is covered by the mode $\boldsymbol{v}_k$. Because the $\boldsymbol{v}_k$ are orthogonal the time-dependent coefficients $\xi_k(t)$ [cf. Eq. (1)] can be easily obtained by projection.

Besides the equivalence of the balls, the symmetry of three-ball cascade juggling patterns is manifested in the phase relation between the balls. The positions of two balls fully determine the position of the remaining one. The "extra information" about this third ball in the form of its trajectory is therefore redundant. The originally six dimensions effectively reduce to four. Thus, in the principal component analysis, one expects the eigenvalues λ_k to drop drastically at $k_0 \leq 4$, that is, $\lambda_{k>k_0} \ll \lambda_{k_0}$ (see also Appendix A). In other words, one expects that it would be sufficient to describe the data set as a maximally four-dimensional system $[\xi_1(t), \ldots, \xi_4(t)]^T$. To illustrate this effect of symmetry we discuss a T-periodic set of piecewise parabolic trajectories defined recursively as

$$\tilde{x}(t) := \begin{cases} t - (T/2 - \tau_h)/2 & \text{for } 0 \leq t < T/2 - \tau_h \\ (T/2 - \tau_h)/2 & \text{for } T/2 - \tau_h \leq t < T/2 \\ -\tilde{x}(t - T/2) & \text{for } t \geq T/2 \end{cases}$$
$$\text{and} \quad \tilde{y}(t) := -\epsilon[\tilde{x}(t)]^2 \quad . \tag{4}$$

T specifies the horizontal periodicity and $\tau_h < T/2$ denotes the time between two consecutive parabolas ($\sim$ time that a hand is loaded with a ball). For this piecewise parabolic juggling model,[1] the entire signal reads $q_{2j+1} := \tilde{x}(t + jT/3)$ and $q_{2(j+1)} := \tilde{y}(t + jT/3)$ for $j = 0, 1, 2$.

As expected, the corresponding principal components vanish for $k \geq 5$ (see Fig. 4). The projections $\xi_k(t)$ are pairwise equivalent by means of the amount of variance λ_k. They are associated with the horizontal and vertical time series. The phase shift between ξ_1 and ξ_2 (and subsequently between ξ_3 and ξ_4) is $\pi/2$ representing the orthogonality of the corresponding eigenvectors (cf. Appendix A).

In analogy with the analysis of the model described above, we investigated the principal components of the recorded juggling patterns. The calculated and normalized eigenvalues for each trial are depicted in Fig. 5 (upper panel). In accordance with the preceding analysis, the last two eigenvalues almost vanished, that is, each pattern essentially reduced to four dimensions. Interestingly, the eigenvalue spectra differed qualitatively between the two experimental conditions. During juggling with a preferred tempo, the largest amount of signal was represented by just two modes ($\lambda_{3,4} \to 0$), whereas for fast juggling the gap between $\lambda_{1,2}$ and $\lambda_{3,4}$ was markedly smaller (Fig. 5, lower panel).

Thus, besides an increase of the overall variance reflecting the fact that performance was worse in the fast condition, the cross-covariance between the vertical and horizontal evolution of the balls increased. The question arose as to the location of this increase in variability in space and time. Since the eigenvalue spectra are based on (cross-)covariances over time – remember that, in Eq. (2), $\langle\cdot\rangle$ denotes the time average – each λ_k represents a different temporal variability. The corresponding eigenvectors or modes can reflect the spatial properties of the system.

Since the results of the following analyses were essentially the same in all trials and subjects, we discuss only two trials in detail. Trial p_2^1 represents juggling in the preferred condition, whereas trial f_1^1 represents juggling in the fast condition. Figure 6 shows the first four eigenvectors $\boldsymbol{v}_{1\ldots4}$ for the two conditions. As is apparent from this figure, the largest amount of variability (the first two modes $\boldsymbol{v}_{1,2}$) was associated with the y-direction. Evidently, the angle between the first two eigenvectors was larger in the fast condition, reflecting an increase in spatial variability. The large angle between eigenvectors $\boldsymbol{v}_3$ and $\boldsymbol{v}_4$ in the preferred condition was of minor importance since the corresponding eigenvalues were

[1] This "model" is in fact a convenient formalization of the ball trajectories based on the physical laws for the free-flight portions and ignoring the non-flight portions

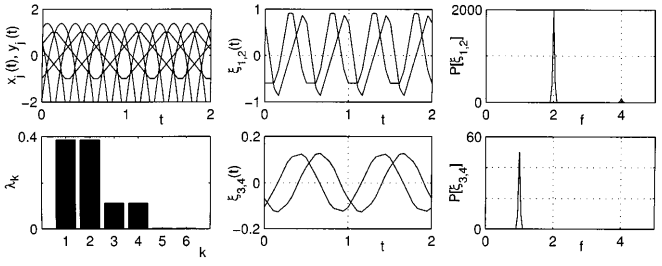

Fig. 4. Principal component analysis of model Eq. (4) with $\epsilon = 2$; time resolution $\Delta t = 8 \times 10^{-3}$ s. The dominant modes account for about 80% of the data ($\sum_{k=1}^{2} \lambda_k \approx 0.8$) and oscillate with the same frequency f_0 as the y_j components. $\xi_{3,4}(t)$ reflect the $x_j(t)$ terms, i.e., they oscillate with $f_0/2$

rather small (cf. Fig. 5). However, their contribution was no longer negligible in the fast condition.

To study the temporal evolution of the balls, we projected the signal onto the individual eigenvectors by means of $\xi_k(t) := [\boldsymbol{v}_k^T \cdot \boldsymbol{q}(t)]$. The projections of the eigenvectors on the experimental time series are shown in Fig. 7 (upper panels). These projections were used to construct the $\xi_2(\xi_1)$ and $\xi_4(\xi_3)$ planes depicted in Fig. 7

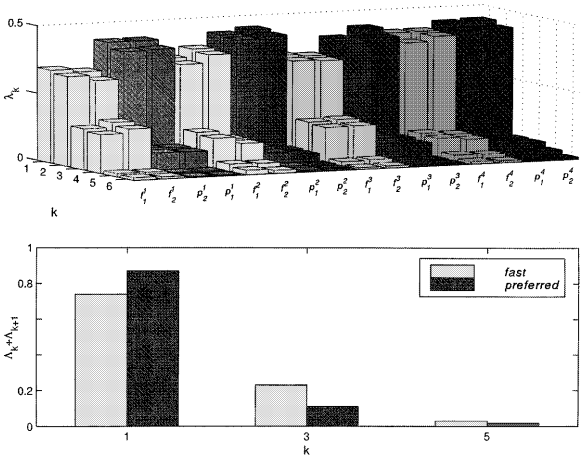

Fig. 5. Principal component analysis of all individuals trials. The six eigenvalues λ_k for all subjects and all conditions are shown; on the ordinate the trials $(f)_j^i$ and $(p)_j^i$ are depicted in the *upper panel* (f fast, p preferred, i subject, j trial number). The averaged values $\Lambda_k := \langle \lambda_k \rangle_{\text{trials}}$ are displayed in the *lower panel*

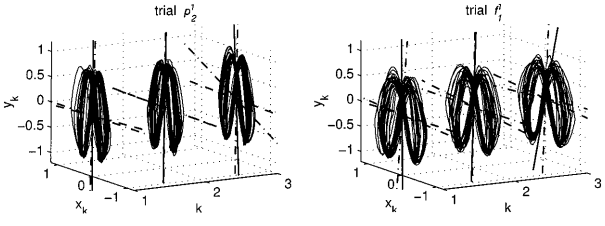

Fig. 6. Eigenvectors $\boldsymbol{v}_j, j = 1, \ldots, 4$ displayed on the subspace of each ball $k = 1, 2, 3$. The *vertical lines* correspond to the first two eigenvectors (*solid* $\boldsymbol{v}_1$, *dash-dotted* $\boldsymbol{v}_2$) and the *horizontal ones* reflect the subsequent two eigenvectors (*dashed* $\boldsymbol{v}_3$, *dash-dotted* $\boldsymbol{v}_4$). *Left panel* preferred condition, *right panel* fast condition

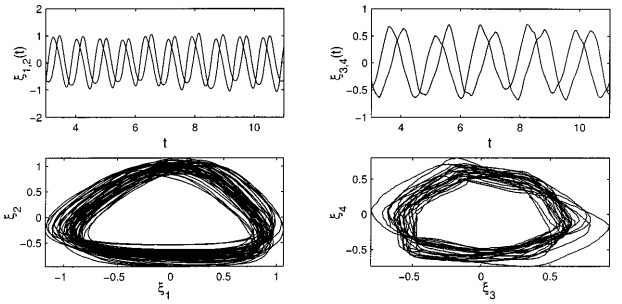

Fig. 7. Data in the fast condition. *Left panels* depict $\xi_{1,2}$, *right panels* depict $\xi_{3,4}$. *Upper panels* projection of the eigenvectors on the data; *lower panels* $\xi_{k+1}(\xi_k)$ plane of projections in the upper panels

(lower panels). Both representations show steady graphs reflecting the strong correlation between the different projections. In good qualitative agreement with the model (Eq. 4; Fig. 8), the projections of the eigenvectors on the data are "jagged", and the corresponding $\xi_{k+1}(\xi_k)$ portraits triagonal or hexagonal.

Similar projections of the eigenvectors on the preferred time series are shown in Fig. 9 (upper panel). Remarkably, the plane representation of the first two projections has a rather circular shape compared to the triangular structure in Fig. 7 (lower left panel). Since $\xi_{1,2}$ were associated with the vertical direction, the trajectories $y_k(t)$ were smoother in the preferred condition. This phenomenon was not present for the x-direction (cf. Figs. 7, 9, lower right panels) where the hexagonal structure of $\xi_4(\xi_3)$ is preserved. It should again be noted that the contribution of the x-direction was of minor

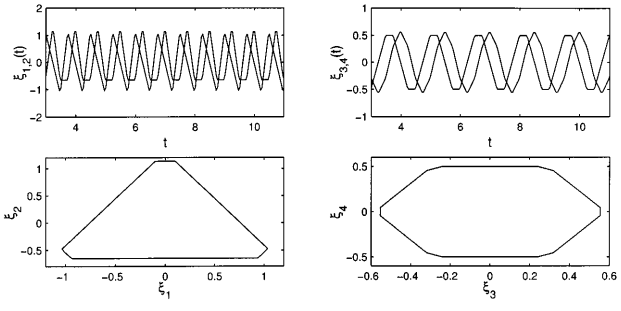

Fig. 8. Model in the fast condition (for legend see Fig. 7). Model Eq. (4) with $T = 1.5$ s, $\tau_h = 0.09$ s

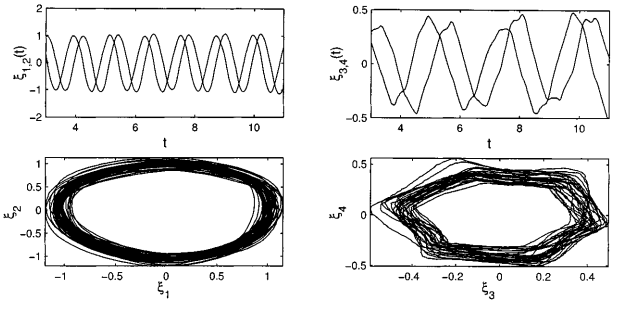

Fig. 9. Data in the preferred condition (for legend see Fig. 7)

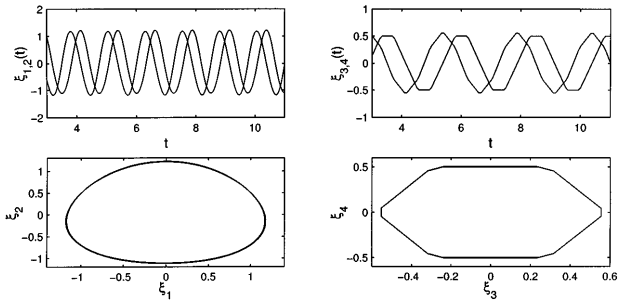

Fig. 10. Model in the preferred condition (for legend see Fig. 7). Model Eq. (4) with $T = 2.5$ s, $\tau_h = 0.15$ s. The vertical components $y_k(t)$ were low-pass filtered (second-order Butterworth at $f_c = 1$ Hz)

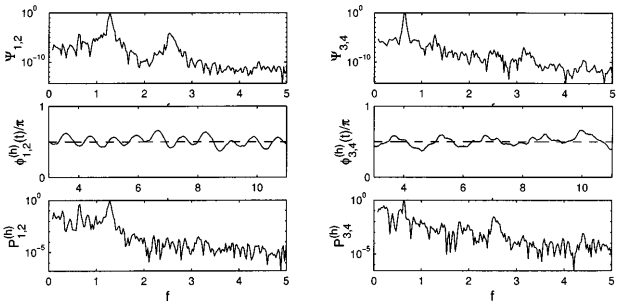

Fig. 11. Data in the fast condition. *Left panels* refer to $\xi_{1,2}$, *right panels* to $\xi_{3,4}$. *Upper panels* logarithmic cross-spectral density plot of the projections in Fig. 7; *middle panels* relative Hilbert phase of these projections; *lower panels* logarithmic power spectral density plot of relative Hilbert phase

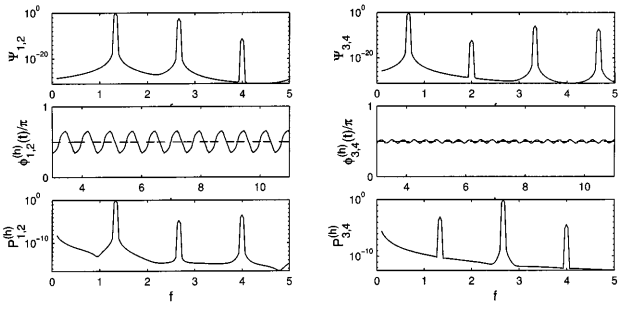

Fig. 12. Model in the fast condition (for legend see Fig. 11). Model Eq. (4) with $T = 1.5$ s, $\tau_h = 0.09$ s (cf. Fig. 8)

importance, given the fact that the corresponding eigenvalues were small. This experimental observation cannot be accounted for by the model as formulated in Eq. (4). Since the change in shape of the $\xi_{k+1}(\xi_k)$ planes can be interpreted in terms of smoothing of the underlying trajectories, the vertical components have to be low-pass filtered (so that catch and throw points become differentiable). The projections thus obtained are in agreement with those of the data (cf. Fig. 9, lower left panel).

To quantify these changes in the shape and smoothness of the time evolution of the eigenvector projections, we analyzed the spectral properties of the dynamics. Therefore, we computed the cross-spectral density $\Psi_{k,l}$ between the pairs of adjacent $\xi_k(t)$

$$\Psi_{k,l}(\omega) := |\mathscr{F}[\xi_k(t)]\mathscr{F}^*[\xi_l(t)]|^2 \ , \tag{5}$$

where $\mathscr{F}[\xi(t)]$ denotes the Fourier transform of $\xi(t)$. In addition, we computed the Hilbert phase $\mathscr{H}(t)$ between these pairs in order to assess the time-dependent relative phase between ξ_k and ξ_l (Rosenblum and Kurths 1998).

$$\mathscr{H}_k(t) := \frac{1}{\pi}\int_{-\infty}^{\infty}\frac{\xi_k(\tau)}{t-\tau}\mathrm{d}\tau \implies$$
$$\phi_{k,l}^{(h)}(t) := \arctan\left\{\frac{\mathscr{H}_k(t)\xi_l(t) - \xi_k(t)\mathscr{H}_l(t)}{\xi_k(t)\xi_l(t) + \mathscr{H}_k(t)\mathscr{H}_l(t)}\right\} \ ; \tag{6}$$

note that $\phi^{(h)}$ is identical to the relative Fourier phase $\phi^{(f)}$ in the case where the signal reads $\xi_k \propto \exp\{i\omega t + i\phi_k\} + c.c.$. Given that the two signals deviate periodically from such a sinusoidal form, the spectral power of $\phi^{(h)}$ shows a distinct peak at the basic frequency. Cross-spectral density results for data and the model in the fast condition are displayed in Figs. 11, 12 (upper panels). The $\Psi_{k,l}$s of the first pair of projections (Figs. 11, 12, upper left panel) showed a strong peak which was identical to the juggling frequency in the y-direction, whereas the $\Psi_{k,l}$s of the second pair of projections (Figs. 11, 12, upper right panel) showed a similarly strong peak which was the same as the frequency in the x-direction. These large peaks reflect the strong frequency locking between $\xi_1(t)$ and $\xi_2(t)$, as well as between $\xi_3(t)$ and $\xi_4(t)$.

The time evolutions of the relative Hilbert phases for data and model in the fast condition are shown in Figs. 11, 12 (middle panels). As was already mentioned, $\phi_{1,2}^{(h)}$ equalled on average $\pi/2$ but displayed pronounced oscillations. The spectral power of the relative Hilbert phase (cf. Figs. 11, 12, lower panels) showed the same dominant frequency as the main cross-spectral frequency (cf. Fig. 12, upper and lower left panels). These oscillations of $\phi^{(h)}$ result from stable periodic deviations from simple sinusoids, suggesting that these deviations occur at fixed points in the $\xi_2(\xi_1)$ representation (Figs. 7, 8, left lower panels). Hence, the representations in question remained steady (cf. Fig. 7). The power spectrum of the Hilbert phase revealed a subharmonic of the dominant movement frequency in the vertical direction (cf. Fig. 11, lower left panel). This frequency, however, was equivalent to the frequency of the horizontal components. Therefore, this subharmonics accounts for the increasing variability along the x-direction that now "creeps into" the first two principal axes.

In contrast with these effects for juggling in the fast condition, Figs. 13, 14 show the spectral analyses for data and model in the preferred condition. All peaks of the spectral densities were markedly shifted to the left compared to the fast condition, indicating a decrease in frequency. Again, the relative Hilbert phase $\phi_{1,2}^{(h)}$ oscillated around $\pi/2$ but the amplitude of this oscillation was markedly reduced in comparison with the fast condition (cf. Figs. 11, 13, middle panels). This low amplitude indicates the presence of rather synchronous sinusoidal trajectories $\xi_1(t)$ and $\xi_2(t)$ (see Fig. 10).

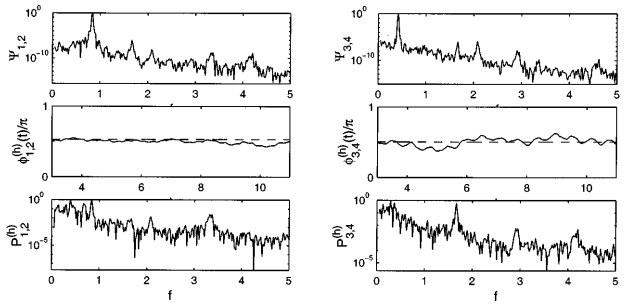

Fig. 13. Data in the preferred condition. *Left panels* refer to $\xi_{1,2}$, *right panels* to $\xi_{3,4}$. *Upper panels* logarithmic cross-spectral density plot of the projections in Fig. 9; *middle panels* relative Hilbert phase of these projections; *lower panels* logarithmic power spectral density plot of relative Hilbert phase

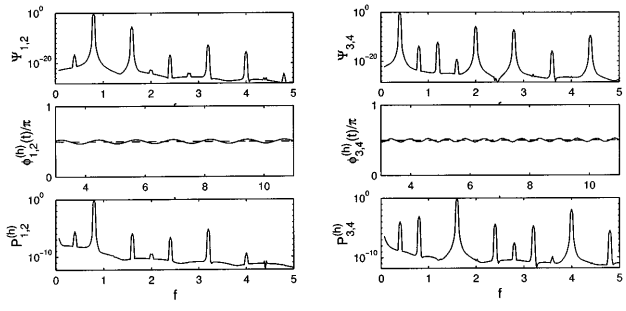

Fig. 14. Model in the preferred condition (for legend see Fig. 13). Model Eq. (4) with $T = 2.5$ s, $\tau_h = 0.15$ s (cf. Fig. 12)

In both conditions, the horizontal components were qualitatively equivalent. Analogous to the vertical parts, the relative Hilbert phase showed small oscillations representing the hexagonal structure of the corresponding $\xi_4(\xi_3)$ planes. Especially for the preferred condition, a broad-banded spectrum was observed at the lower frequencies which, however, could be neglected given that the corresponding eigenvalues were very small.

3.2. Temporal correlations

Despite the marked differences in smoothness of the movement trajectories in both conditions, the timing properties were quite similar. That is, frequency and phase locking were equally present in fast and preferred juggling. In the former case, however, the performance was worse so that one would expect at least an increase of the timing variability. Increasing variability implies increasing timing errors that, given the task constraints, can be expressed in terms of deviations of the $2\pi/3$ phase difference between the balls. The deviations predominantly occurred at distinct locations as shown in Figs. 7 and 8. These points define the different geometrical properties of the $\xi_{k+1}(\xi_k)$ representations. For example, $\xi_4(\xi_3)$ showed a hexagonal structure indicating six important events, i.e., two events per ball per cycle, whereas $\xi_2(\xi_1)$ hinted at the presence of a single distinct event per ball per cycle (triangular structure). All these events showed pronounced discontinuities in the derivatives of $\xi_k(t)$ with respect to time. Thus, they did not occur along the parabolic part of the trajectories. Since these events are more or less fixed in phase and position, it is most likely that they are associated with the throws and the catches. A closer comparison between the temporal evolutions $\xi_k(t)$ and the corresponding $x_j(t)$ and $y_j(t)$ confirmed this expectation. Explicitly, the most important events for the dynamics of ξ_1 and ξ_2 were the catch points. The higher modes $\xi_{3,4}$ were additionally affected by the throw points. Forthcoming studies of temporal correlations can therefore focus exclusively on these events. Notice that these discrete events emerged from the preceding analyses that involved no a priori knowledge of the juggling pattern.

Besides the locations of the throws and the catches, a complete determination of the parabolic part of the trajectories requires either the initial force (velocity) of the throw or the location of the parabola's zenith. Therefore, we computed time intervals between consecutive zeniths, consecutive catches and consecutive throws by, or referring to, the same hand (i.e., left, right). As shown in Fig. 15, the normalized variances of the time intervals between consecutive catches by the same hand were consistently larger in the fast condition than in the preferred condition. Throw and zenith intervals did not show such a significant difference between the two conditions. This result can be readily explained: Every distinct point $t_a \ldots t_c$ contributes to the temporal variability of the overall cycle. Consequently, the variance of the very last point, i.e., the catch, includes the variability of all previous ones (throw, zenith), at least to some extent. All previous errors are combined in the point of catch that, with its additional own variability, shows the largest total variance.

The variance $s_0^2(\xi) := E(\xi^2) - E(\xi)^2$ with $E(\cdot)$ as expectation value of ξ reflects the amount of errors but it disregards any mechanism of error correction. To gain insight into such mechanisms, we considered the first three lag covariances $s_\tau^2(\xi) := E([\xi_t - E(\xi)][\xi_{t+\tau} - E(\xi)])$. The lags $\tau = 0, \ldots, 3$ refer to the consecutive balls (e.g., lag-zero: ball$_1$, lag-one: ball$_2$, lag-two: ball$_3$, lag-three: ball$_1$, etc.). Again, the most dominant lag-covariances were found at the catch point because the point of maximal variance requires larger error corrections. The increase of variance was accompanied

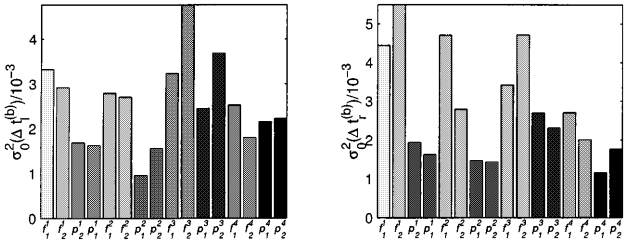

Fig. 15. Normalized variances $\sigma_0^2 := s_0^2(\Delta t^{(b)})/\overline{\Delta t^{(b)}}$ of the intervals between the catches for all individuals trials. *Left panel* catches with left hand: *right panel* catches with right hand

by an increase of the absolute covariance. For an immediate comparison between the different points of interest, we therefore used an appropriate normalization. Explicitly, we compared lag correlations of the form $\gamma_\tau := \sigma_\tau^2/\sigma_0^2 \equiv s_\tau^2/s_0^2$ denoting relative serial error corrections. Analogous to the findings of Wing and Kristofferson (1973) regarding self-paced isochronous rhythmic movements, we found markedly negative lag-one correlations in the range $-0.5 \leq \gamma_1 \leq 0$ as shown in Fig. 16. As this effect was symmetric for both hands, it suggests that errors in the phase relation between consecutive balls are immediately corrected by the catches. The higher lags were centered around zero and can thus be neglected as possible correction mechanisms. Interestingly, the lag-one correlations were only significantly negative for the catches. For the throws and the zeniths, all serial lag correlations were negligible. That is, deviations in the timing of the throw do not affect timing of the subsequent throw whereas the catch is used to correct for the proper phase relation between the balls. This correction of relative errors is independent of the cycle frequency.

In a manner analogous with the temporal properties of the system, we finally studied variances and correlations of the spatial locations of throw, zenith and catch. At the throw points, we further computed the balls' initial velocities. For all computed variables, the variances for the preferred and the fast condition were not significantly different. In detail, no structure was observed in the variance of x- or y-directions of the position of throws, zeniths, or catches, nor in the x- or y-direction of the velocity at the throws. Similarly, the lag correlations did not hint at any spatial error correction mechanism between consecutive balls, i.e. no particular auto-correlation patterns could be discerned in these positions and velocities. However, the findings of Beek and Van Santvoord (cf. spatial clock; Van Santvoord and Beek 1996) indicate the presence of some mechanism that pronounces distinct points in space in addition to the discontinuities of throwing and catching. Since the ball flight trajectories and, in particular, their zeniths, are determined by the location of the throw and its force, one can expect significant cross-correlations between the corresponding variables, and possibly correlations at different lags. This analysis, however, is beyond the scope of the present study.

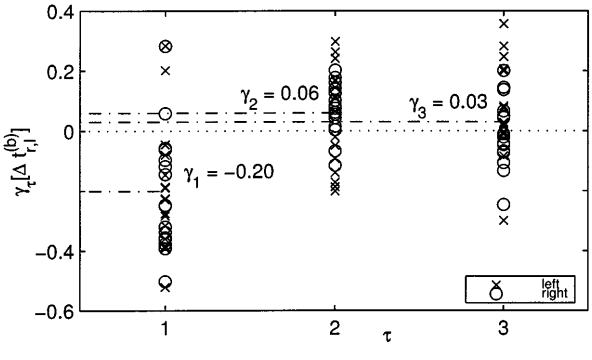

Fig. 16. Serial correlations $\gamma_\tau := \sigma_\tau^2/\sigma_0^2 \equiv s_\tau^2/s_0^2$ at the point of catch $t^{(c)}$. On average, the lag-one correlation is negative ($\bar{\gamma}_1 = -0.2$) whereas the higher lags are not significantly different from zero, i.e., $\bar{\gamma}_{2,3} \approx 0$

4 Discussion

In the present article, we showed analytically that the inherent symmetries of three-ball cascade juggling patterns imply a reduction of the dimensionality of these patterns. This theoretical result was corroborated experimentally. Principal component analysis revealed that the six-dimensional ball pattern can always be treated as a maximally four-dimensional system. In the fast condition, all these four dimensions were needed to reconstruct the signal. In the preferred condition, however, vertical and horizontal components were almost perfectly correlated, i.e., $x(t)$ determined $y(t)$ and vice versa. As a consequence, the system's dimensionality reduced further to two in this case. In control theoretical terms this indicates that, in the preferred condition, the system has to accommodate fewer dimensions, implying a strong reduction of the control problem. It is important to note that the experimental manipulation of movement frequency from fast to preferred is completely unspecific to this reduction, i.e., it does not entail it. Thus, a change in detail (frequency) causes a qualitative change in the movement as a whole (dimensionality of the control space), in a manner already intuited by Bernstein (1984 p. 84). For both conditions, the first two eigenvalues $\lambda_{1,2}$, that is, the two most important modes, were always associated with the y-direction. This implies that the main direction of control is along the (gravitational) vertical, which is consistent with the previous findings of Van Santvoord and Beek (1996). The corresponding cross-spectral densities and Hilbert phases revealed that the timing properties, i.e., the 1:2 frequency locking and the $2\pi/3$ phase locking were not affected by a change in tempo. For the fast condition, however, the power spectra of the relative Hilbert phase between ξ_1 and ξ_2 showed an increased importance of the horizontal components which coincided with increasing eigenvalues $\lambda_{3,4}$, that is, a higher dimensionality of the system (two $\rightarrow$ four). This finding might be associated with the decrease in angle of release in the fast condition.

Besides these global and time-dependent aspects, a further important change in the movement pattern was located in space and time. Depending on the condition, the smoothness of the ball trajectories changed markedly at the catch points. This reflects the increasing difficulty at higher circulation speeds to precisely match the hand velocity vector to that of the ball. Thus, the degree of smoothing of the projections $\xi_{1,2}(t)$ can be taken as an index of the quality of task performance. An equivalent change of smoothness in the horizontal direction was not observed. The projections $\xi_4(\xi_3)$ always showed hexagonal shapes with the angles related to the catch points (left and right hand). Concerning the timing correction, juggling frequency had also a large effect on the variance of catch-catch cycles. Combined with the

relatively large spatial variance, this fact underscores that the significance of the catches is in correcting errors in the timing of the act (i.e., the stabilization of the $2\pi/3$ phase difference between the balls). The increase of temporal variability is corrected by means of the observed negative lag-one serial auto-correlation. That is, errors in the phase relation between consecutive balls are immediately compensated by the catches. Higher lags, i.e., forthcoming catches, are not relevant for this control mechanism. It can be expected that the spatial variability of the catch is exploited to reduce the aforementioned temporal variability in the catch-catch cycles. The exact form of this control mechanism, however, remains an issue for further study.

Negative lag-one correlations have been frequently observed in the context of the unimanual, unpaced performance of rhythmic movements. To account for such correlations, Wing and Kristofferson (1973) formulated a model that presupposes two hierarchical levels involving an internal timekeeper (clock) and some motor delay. This model addresses statistical aspects (variability and correlations) of temporal structures. The juggling pattern, however, also depends on spatial constraints. Further modeling should therefore account for the explicit spatiotemporal forms of $x_j(t)$ and $y_j(t)$. Equation (4) does not elucidate all spatiotemporal phenomena, but describes important features of three-ball cascade juggling such as its inherent symmetry and the physical nature of ballistic throws. In a recent study by one of us, it has been shown how to incorporate certain timing aspects into oscillatory dynamical systems (Daffertshofer 1998). In particular, negative serial correlations can be generated in a system of coupled oscillators by introducing additional stochastic forces. Thus, an extension towards stochastic dynamical models allows one to account for both the stability properties and the variability in the timing. Various aspects of variability can now be addressed coherently from the perspective of coordination dynamics. The results presented in this paper merit the conclusion that valuable insights into motor performance can be gained by studying its spatiotemporal variability in detail. This, however, requires appropriate methods of analysis that do not involve any a priori assumptions with regard to the system under investigation. The methods applied in the present paper are examples of such unbiased tools since they take the entire spatiotemporal evolution of the movement pattern into account.

Appendix

A. Symmetries

In this appendix, we consider the consequences of the inherent symmetries of juggling for the number of relevant principal components. Since juggling is an essentially rhythmic activity, we study a T-periodic function $f(t) = f(t+T)$. For the sake of generality we do not further specify the explicit form of $f = f(t)$. Without any restrictions, we assume $T \equiv 1$ and subtract the mean of $f(t)$, i.e., we consider the case $\langle f(t) \rangle = 0$. Regarding the periodic nature of $f(t)$, we compute its corresponding Fourier transform. Explicitly, the Fourier series reads

$$f(t) = \sum_{n=1}^{\infty} \{a_n \sin(2\pi n t) + b_n \cos(2\pi n t)\} \ . \tag{7}$$

The symmetries in juggling can be expressed in terms of phase locking between the balls. With identical balls, we thus treat the case of different sets of functions $f(t)$ that are pairwise shifted in phase by $2\pi/3$.

At first, the signal is composed of three components, i.e., we have

$$\boldsymbol{q}(t) = \sum_{k=0}^{2} f\left(t + \frac{k}{3}\right) \boldsymbol{e}_k \ , \tag{8}$$

where $\boldsymbol{e}_k$ are the unity vectors in $\mathbb{R}^3$. Given the symmetry of the signal the corresponding covariance matrix becomes

$$\underline{\boldsymbol{R}} = \frac{1}{3\sigma^2} \begin{pmatrix} \sigma^2 & \varsigma^2 & \varsigma^2 \\ \varsigma^2 & \sigma^2 & \varsigma^2 \\ \varsigma^2 & \varsigma^2 & \sigma^2 \end{pmatrix}$$
$$\Longrightarrow \quad \lambda_{1,2} = \frac{\sigma^2 - \varsigma^2}{3\sigma^2} \quad \text{and} \quad \lambda_3 = \frac{\sigma^2 + 2\varsigma^2}{3\sigma^2} \ . \tag{9}$$

The two different covariances can be calculated as

$$\sigma^2 = \int_0^1 f(t)^2 \mathrm{d}t = \frac{1}{2} \sum_{n=1}^{\infty} \{a_n^2 + b_n^2\}$$
$$\varsigma^2 = \int_0^1 f(t) f(t + 1/3) \ \mathrm{d}t = -\frac{\sigma^2}{2} \ . \tag{10}$$

Thus, the covariance matrix has only two non-vanishing but degenerated eigenvalues $\lambda_{1,2} = 0.5$. Orthogonalization of the corresponding eigenvectors yields

$$\boldsymbol{v}_1 = \begin{pmatrix} -2 \\ 1 \\ 1 \end{pmatrix}, \ \boldsymbol{v}_2 = \begin{pmatrix} 0 \\ 1 \\ -1 \end{pmatrix}, \ \text{and} \ \boldsymbol{v}_3 = \begin{pmatrix} 1 \\ 1 \\ 1 \end{pmatrix} \ . \tag{11}$$

This orthogonality $\boldsymbol{v}_1 \perp \boldsymbol{v}_2$ leads to periodic projections $\xi_{1,2}(t)$ that are phase-shifted by $\pi/2$, i.e.,

$$\xi_k(t) = \xi_k(t+1) \quad \wedge \quad \xi_2(t) = \xi_1\left(t + \frac{1}{4}\right) \ . \tag{12}$$

Next, we extend the number of dimensions of the signal to six by introducing a $T/2$-periodic function $g(t) = g(t + T/2)$. This property is actually present in the studied data set. Again, we use the symmetry of the system and the aforementioned results in three dimensions and obtain

$$\underline{\boldsymbol{R}} \propto \begin{pmatrix} \underline{\boldsymbol{R}}^{(h)} & \underline{\boldsymbol{R}}^{(gh)} \\ \underline{\boldsymbol{R}}^{(gh)} & \underline{\boldsymbol{R}}^{(g)} \end{pmatrix} \ . \tag{13}$$

Each sub-matrix $\underline{\boldsymbol{R}}^{(\alpha)}$ has equivalent symmetries as (9), that is, the diagonal elements are $\sigma^2_{(\alpha)}$ and all off-diagonal components read $-\sigma^2_{(\alpha)}/2$. Thus, this combined covariance matrix $\underline{\boldsymbol{R}}$ has two vanishing eigenvalues $\lambda_{5,6} = 0$ and two degenerated sets

$$\lambda_{\substack{1,2 \\ (+);\,(-)}}^{\substack{3,4 \\ }} = \frac{1}{4} \left[1 \pm \sqrt{\frac{\left(\sigma^2_{(h)} - \sigma^2_{(g)}\right)^2 + 4\sigma^2_{(gh)}}{\left(\sigma^2_{(h)} + \sigma^2_{(g)}\right)^2}} \right] \ . \tag{14}$$

As a result, the originally six-dimensional system is reduced to four dimensions. In the case of phase-locking between $f(t)$ and $g(t)$, the cross-covariance $\sigma^2_{(gh)}$ tends to zero based on the orthogonality of the trigonometric functions. Thus, if the individual variances $\sigma^2_{(h)}$ and $\sigma^2_{(g)}$ are identical, both eigenvalues will become $\lambda_{(+);(-)} \to 1/4$. On the other hand, if one variance vanishes, e.g., $\sigma^2_{(h)} \to 0$, the corresponding eigenvalue will vanish as well ($\lambda_{(-)} \to 0$). In this case, the system essentially becomes two-dimensional.

References

Beek PJ (1989) Juggling dynamics. PhD thesis, Vrije Universiteit Amsterdam

Beek PJ, Lewbel A (1995) The science of juggling. Sci Am 273: 92–97

Beek PJ, Turvey MT (1992) Temporal patterning in cascade juggling. J Exp Psychol Hum Percept Perform 18:934–947

Beek PJ, Van Santvoord AAM (1992) Learning the cascade juggle: a dynamical systems analysis. J Mot Behav 24:85–94

Benzi R, Sutera A, Vulpiani A (1981) The mechanism of stochastic resonance. J Phys A 14:L453

Bernstein NA (1984) The problem of the interrelation of coordination and localization. In: Whiting HTA (ed) Human motor actions: Bernstein reassessed. North-Holland, Amsterdam, pp 77–120

Daffertshofer A (1998) Effects of noise on the phase dynamics of nonlinear oscillators. Phys Rev E 58:327–338

Fuchs A, Kelso JAS, Haken H (1992) Phase transitions in the human brain: spatial mode dynamics. Int J Bifurc Chaos 2:917–939

Gardiner CW (1990) Handbook of stochastic methods, 2nd edn. Springer, Berlin Heidelberg New York

Haas R (1995) Bewegungserkennung und Bewegungsanalyse mit dem synergetischen Computer. PhD thesis, Universität Stuttgart, Germany

Haggard P, Wing A (1997) On the hand transport component of prehensile movements. J Mot Behav 29:282–287

Haken H (1983) Synergetics. An introduction, 3rd edn. Springer, Berlin Heidelberg New York

Haken H (1988) Information and self-organization. Springer, Berlin Heidelberg New York

Haken H (1996) Principles of brain functioning. A synergetic approach to brain activity, behavior, and cognition. Springer, Berlin Heidelberg New York

Hu Gang, Daffertshofer A, Haken H (1996) Diffusion of periodically forced Brownian particles moving in space-periodic potentials. Phys Rev Lett 76:4874–4877

Jung P, Hänggi P (1991) Amplification of small signals via stochastic resonance. Phys Rev A 44:8032

Karhunen K (1946) Zur spektralen Theorie stochastischer Prozesse. Ann Acad Sci Fenn A1, Math Phys 37

Kelso JAS (1995) Dynamic patterns. The self-organization of brain and behavior. MIT Press, Cambridge, Mass

Oja E (1992) Principal components, minor components, and linear neural networks. Neural Netw 5:927–935

Rosenblum M, Kurths J (1998) Analysing synchronization phenomena from bivariate data by means of the Hilbert transform. In: Kantz H, Kurths J, Mayer-Kress G (eds) Nonlinear analysis of physiological data. Springer, Berlin Heidelberg New York, pp 91–99

Shannon CE, Weaver W (1949) The mathematical theory of communication. University of Illinois Press, Urbana Ill

Thaut MH, Miller RA, Schauer LM (1998) Multiple synchronization strategies in rhythmic sensorimotor tasks: phase vs period correction. Biol Cybern 79:241–250

Van Santvoord AAM (1995) Cascade juggling: learning, variability and information. PhD thesis, Vrije Universiteit Amsterdam, CopyPrint 2000

Van Santvoord AAM, Beek PJ (1996) Spatiotemporal variability in cascade juggling. Acta Psychol 91:131–151

Vorberg D, Wing AM (1996) Modeling variability and dependence in timing. In: Heuer H, Keele SW (eds) Handbook of perception and action, vol 2. Academic Press, London, pp 181–261

Wackerbauer R (1998) Noise-induced stabilization of one-dimensional discontinuous maps. Phys Rev E 58:3036–3044

Wing AM, Kristofferson AB (1973) Response delays and the timing of discrete motor responses. Percept Psychophys 14:5–12